Nappe Oscillations on Free-Overfall Structures: Experimental Analysis

Maurine Lodomez[1]; Michel Pirotton[2]; Benjamin Dewals[3]; Pierre Archambeau[4]; and Sébastien Erpicum[5]

Abstract: Under relatively low heads, the occurrence of nappe oscillation, also known as nappe vibration, may be observed on hydraulic structures with a free overfall, such as weirs, crest gates, and fountains. This phenomenon is characterized by oscillations of the thin flow nappe cascading downstream of the crest and results in a disturbing noise production that increases the environmental and societal impacts of the hydraulic structure. Given limited information available regarding the physical processes involved in this phenomenon, a detailed investigation has been undertaken to characterize the flow for free-overfall structures where nappe oscillation may be of concern. The research is conducted on a prototype-scale linear weir model (weir length of 3.5 m and a fall height of 3 m) using high-speed cameras and audio equipment to characterize the nappe oscillation. The paper presents the quantitative characteristics of the nappe oscillation gained from images and sound analysis, especially in terms of frequency, for aerated and confined nappe configurations. **DOI: 10.1061/(ASCE)HY.1943-7900.0001420.**

Author keywords: Flow visualization; Hydraulic models; Nappe vibration; Oscillatory flows; Sound measurements; Spillway.

Introduction

Nappe oscillations have been identified as an undesirable and potentially dangerous phenomenon in the case of flow over a gate (Naudascher and Rockwell 1994; USBR 1964). Their occurrence on this widespread type of structure has been attributed in part to the interaction between the flow and the enclosed air pocket bounded by the gate and the nappe (Naudascher and Rockwell 1994). Indeed, adding splitters to the gate crest to divide the nappe and thus venting the air pocket has been successful in mitigating nappe oscillation problems.

In addition to gates, nappe oscillations have also been observed on free-surface weirs, including labyrinth weirs, even with an aerated air pocket behind the nappe (Crookston et al. 2014; Crookston and Tullis 2013; Metropolitan Water, Sewerage, and Drainage Board 1980; Schwartz 1966). However, such dam safety structures typically operate less frequently than overflow gates used as regulating structures. Contrary to the case of gates, the use of splitters is not recommended on free-surface spillways because it reduces the discharge capacity of the weir and favors floating debris collection. As a consequence, the low number of free-surface weirs leading to nappes oscillation has promoted the implementation of case-by-case countermeasures, such as an increase in the crest roughness or a modification of the crest profile (Metropolitan Water, Sewerage, and Drainage Board 1980).

Besides these practical considerations, a review of the scientific literature shows that nappe oscillations have been subject to various theoretical and experimental modeling over the last 70 years. Squire (1953) investigated the breakup of thin falling liquid films of constant thickness due to the growth of oscillations. He showed that the surface tension is a dominant factor in the stability analysis of the liquid film and in the determination of the wavelength of the oscillations that cause its breakup. Schwartz (1966) discussed the similarities between edgetones and nappe oscillations phenomena. The sensitivity of nappe oscillations to the crest weir roughness led the author to suggest the stability of the boundary layer on the weir crest as a significant nappe oscillation parameter. He also supported the integer-plus-one-quarter criterion, equivalent to the one proposed by Curle (1953) for the jet-edge system. This criterion considers that the pressure changes generated in the surrounding air by the nappe come into phase with the pressures exerted on individual nappe elements when the number of wavelengths contained in the length of the nappe is an integer plus one-quarter. Binnie (1972) experimentally studied thin sheets of water flowing vertically along a 0.305- to 0.61-m-high chute from 0.2- to 1.6-mm-wide slots created in a pressurized tube. The disintegration of this vertical sheet falling at atmospheric pressure on both sides was examined and related to Weber number at the breakup while, in case of an air pocket trapped on one side of the sheet, oscillation frequencies were evaluated. The frequency was measured with a microphone connected to an oscilloscope and was found to vary from 2 to 33 Hz. Based on these experimental

[1]Ph.D. Student, ArGEnCo Dept., Research Group of Hydraulics in Environmental and Civil Engineering, Univ. of Liege, Quartier Polytech, Allée de la Découverte 9, Bat B52/3 +1, B-4000 Liège, Belgium (corresponding author). E-mail: m.lodomez@ulg.ac.be

[2]Professor, ArGEnCo Dept., Research Group of Hydraulics in Environmental and Civil Engineering, Univ. of Liege, Quartier Polytech, Allée de la Découverte 9, Bat B52/3 +1, B-4000 Liège, Belgium. E-mail: michel.pirotton@ulg.ac.be

[3]Associate Professor, ArGEnCo Dept., Research Group of Hydraulics in Environmental and Civil Engineering, Univ. of Liege, Quartier Polytech, Allée de la Découverte 9, Bat B52/3 +1, B-4000 Liège, Belgium. E-mail: B.Dewals@ulg.ac.be

[4]Research Associate, ArGEnCo Dept., Research Group of Hydraulics in Environmental and Civil Engineering, Univ. of Liege, Quartier Polytech, Allée de la Découverte 9, Bat B52/3 +1, B-4000 Liège, Belgium. E-mail: pierre.archambeau@ulg.ac.be

[5]Assistant Professor, ArGEnCo Dept., Research Group of Hydraulics in Environmental and Civil Engineering, Univ. of Liege, Quartier Polytech, Allée de la Découverte 9, Bat B52/3 +1, B-4000 Liège, Belgium. E-mail: S.Erpicum@ulg.ac.be

Note. This manuscript was submitted on December 6, 2016; approved on August 24, 2017; published online on January 2, 2018. Discussion period open until June 2, 2018; separate discussions must be submitted for individual papers. This paper is part of the ***Journal of Hydraulic Engineering***, © ASCE, ISSN 0733-9429.

results, Binnie (1974) theoretically investigated the instability of a vertically falling water sheet with disturbances due to resonance with the confined air pocket. Although this theory can explain some characteristics of the phenomenon, it does not specify which of an infinite number of modes and frequencies, theoretically defined, is likely to occur. Casperson (1993a) experimentally examined the nappe oscillations occurring on Dunedin's fountains (New Zealand) and theoretically established integrodifferential equations of the sheet waveforms and oscillation frequency whose solutions are in agreement with the experimentally observed behavior. The experiments were performed for a nearly vertical flow with fall heights varying from 0.41 to 0.80 m and frequency in the range of 5–12 Hz. In a later study, Casperson (1994) derived a stability criterion based on this set of equations by exploring the dependence of the flow rate with the fountain height for various depths of air chamber, initial velocity, and air velocity. In addition, this author (Casperson 1993b) proposed the following equation of the oscillation frequency f:

$$f = \frac{m + 0.25}{\frac{v_0}{g}\left[(1 + 2gL/v_0)^{1/2} - 1\right]} \tag{1}$$

where m = integer; v_0 = initial velocity; and L = fall height. He recognized that the confined air pocket behind the water sheet plays a central role in providing a feedback mechanism as suggested in Naudasher (1965), Petrikat (1958), and Schwartz (1964). In addition to this feedback, he attributed the mechanism of amplification required to initiate the instability to shear forces that occur at the interface between the falling water and air, in a Kelvin-Helmholtz mechanism (Helmholtz 1868). Chanson (1996) suggested a pressure discontinuity at the weir crest as the cause of the phenomenon, with an origin of the oscillations at the crest. Schmid and Henningson (2002) theoretically investigated the stability of a vertically falling water sheet enclosing an air pocket by applying a multimodal approach. The developed multimodal stability analysis demonstrated a strong amplification of the total energy and the pressure difference in the air pocket for integers of the fall time. These results were in agreement with experimental data with a fall height and slot width varying, respectively, between 0.31 and 0.7 m and 1.5 and 2 mm. The frequencies experimentally reported were between 4 and 9.85 Hz. This study suggests that the nappe oscillation phenomenon is governed not by a single mode, but a linear interaction of several modes. In the same way, Sato et al. (2007) concluded that the nappe oscillations occur under conditions where the work done by the water sheet on the air pocket reaches a maximum taking place when the product of the frequency and the falling time is an integer plus one-quarter. In addition, Sato et al. (2007) experimentally found that the pressure fluctuations frequency is identical to the frequency of the confined water sheet oscillations, initiated through a slot of 1.3 or 3.1 mm. The falling height of the experimental apparatus varied from 0.47 to 0.62 m, and the frequencies were recorded between 5.3 and 17.4 Hz. De Rosa et al. (2014) investigated theoretically the mutual influence of the air pocket behind the nappe with the nappe interface that generates self-induced forces by recasting the nappe global behavior as a driven damped spring-mass oscillator whose mass is that of the liquid sheet, and the equivalent stiffness of the spring is that of the air inside the enclosure. Through a modal and a nonmodal linear approach, this unsteady global analysis examined both the dynamics and the energy aspect. The modal analysis indicated that the system is characterized by low frequency, related to the quasi-constant spacing of the imaginary part of the eigenvalues (Schmid and Henningson 2002) and high-frequency oscillations, related to a global spring-mass oscillator model. Finally, a substantial result of this study is a stability criterion "based on the ansatz that the system is stable if the crossing time of a perturbation over the whole length of the domain is shorter than the period of the spring mass oscillator." Girfoglio et al. (2017) further studied the global dynamic behavior of nappe oscillations of a vertical thin sheet interaction with an air pocket in the presence of surface tension effects. Key findings of the global dynamics analysis are the agreement with experimental data of the literature and the definition of the two characteristic frequencies, that of the spring-mass behavior and that of the capillarity wave traveling over the sheet.

Recently, following the nappe vibration problems experienced after the rehabilitation of the Linville Land Harbor Dam, new experimental investigations were undertaken at the Utah Water Research Laboratory on large-scale free-surface weirs (Anderson 2014; Crookston et al. 2014). It is worth noticing that the main problem of the nappe oscillations occurring on a dam emergency structure is the noise, which negatively affects people living close to these dams. These tests suggest that the origin of the instability most likely occurs at the weir crest. Indeed, the waves resulting in the oscillations are observed directly after the flow separation from the weir crest (even for unconfined nappes) and roughness modifications of the weir affect the oscillations occurrence.

It can be concluded from literature that the nappe oscillation is a complex hydraulic process in which more than one mechanism may initiate oscillation, provide feedback, and/or sustain the oscillation. The majority of experimental studies performed to date considered thin vertically falling sheets of water originating from a thin slot in a pressurized tube with limited fall heights (lower than 1 m) and air pocket trapped behind the nappe. Oscillations frequency is the main parameters used to characterize the phenomenon. From a theoretical perspective, the models presented in the literature require the presence of this air pocket behind the nappe to explain the oscillations development. In contrast, it is known and reported by some authors (Anderson 2014; Sato et al. 2007) that nappe oscillations can occur on free-surface weirs (i.e., for nappe originating horizontally from a crest), even if the nappe is fully aerated.

In this respect, the experimental study presented in this paper has been undertaken on a 1:1 physical model of a free-surface linear weir (3-m-high chute) in confined and unconfined nappe conditions with the aim of getting data in real-size chute conditions for dam emergency structures prone to be subject to nappe oscillations. The paper first depicts the experimental set-up and the methodology developed to characterize the frequency and noise intensity of the nappe oscillations by means of sound and image analysis. Second, the results are analyzed to characterize the noise evolution with the discharge and the downstream impact conditions, and also to assess the effect of nappe confinement. Comparison of these new experimental results with ones from the literature enables to highlight differences, but also similarities, in the observed oscillations characteristics.

Experimental Set-Up

Weir Model

A prototype-scale linear weir was constructed at the engineering hydraulics laboratory at the University of Liège. It is made of an elevated reservoir supplying two identical weirs with a 3.5-m-long crest and a 3.0-m-high chute downstream (Fig. 1). The reservoir is fed by two pumps delivering up to 0.25 $m^3 \cdot s^{-1}$ through perforated pipes parallel to the crest and located at the bottom of the reservoir. The discharge is measured with an electromagnetic flow meter installed on the supply pipe, with an accuracy better than 0.5% of the

(a)

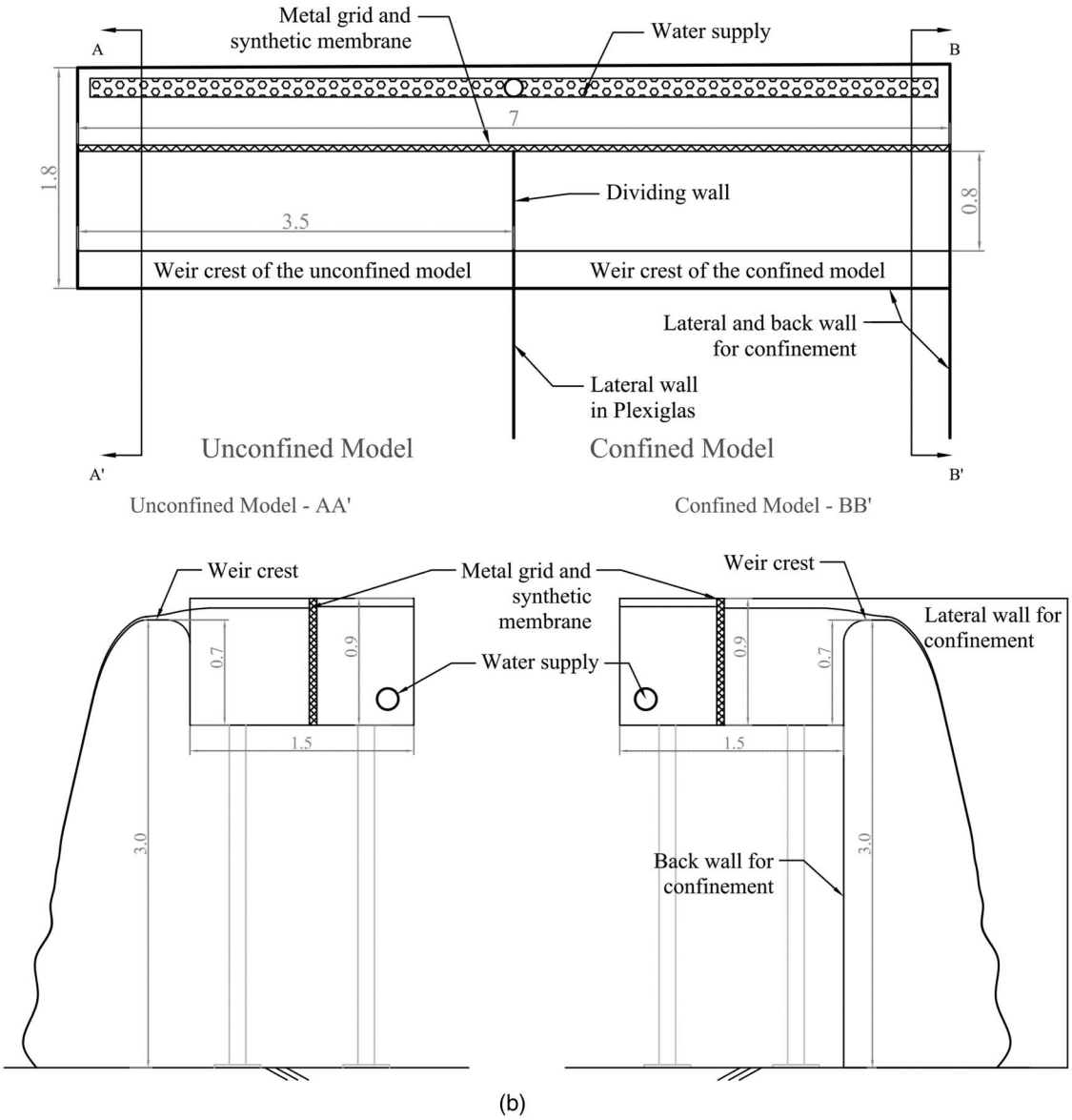

(b)

Fig. 1. Experimental set-up: (a) experimental set-up with an unconfined nappe configuration; (b) plan view of the experimental facility and cross sections of the unconfined and the confined models (dimensions in meters)

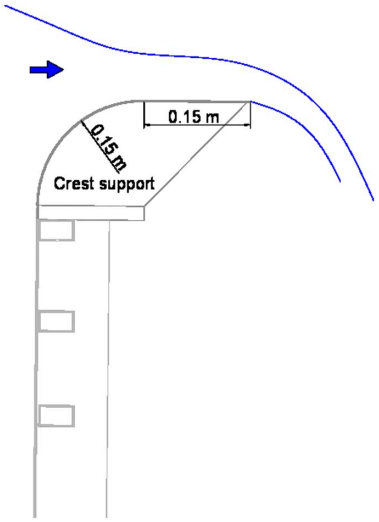

Fig. 2. Crest weir details

full scale according to the calibration sheet of the device. The reservoir is equipped with a metal grid and a synthetic membrane ensuring uniform velocity distribution upstream of the weirs. The weir crest, located at the downstream extremity of the reservoir, is a 0.30-m-thick quarter round crest with a radius of 0.15 m (Fig. 2). These are typical prototype dimensions for reinforced concrete weirs. The air pocket behind the nappe can be confined or unconfined. As illustrated in Fig. 1(b), the weir located on the left side of the reservoir is confined between two lateral walls and a back wall, one lateral confinement wall being transparent (Plexiglas) and the others made of black multiplex panels. The weir on the right side is unconfined, also called aerated in the following, except on the shared lateral side. The weirs can be isolated so as to only operate one at a time, as illustrated in Fig. 1(a).

Sound Analysis

To get data on the noise produced by the oscillations, a free-field microphone MC212 (01dB-Metravib, Limonest, France), was placed along the centerline of the weir crest, 2.5 m downstream in front of the falling nappe. After testing several positions around the model, it was found that placing the microphone in front of the nappe makes it possible to obtain, on the one hand, the sound that is least affected by ambient noise, in particular the noise generated by the pumps, and, on the other hand, the most direct sound produced by the oscillations. This noise was assumed to arise from the air-water interaction. Indeed, although the impact is also a source of noise, Anderson (2014) showed that the modification of the impact by using a foam pad on apron did not affect the sound characteristics. This has also been tested in this study and discussed subsequently.

The microphone has a frequency range between 6 Hz and 20 kHz and a dynamic range between 15 and 146 dB. The recording and analysis of audio data were carried out by means of the *dBFA* software suite, which supplies the autospectrum of the audio signal by applying a narrowband analysis of the audio signal. The audio autospectrum provides an image of the sound level for each frequency of the noise. This spectral analysis is based on a classical periodogram or Gabor analysis, with the selection of an overlap and a weighting window (*01dB-Metravib*). The result, named sound level or intensity in the following, is expressed in decibels and is equal to $20\log[|G_{xx}|/(2\times10^{-5})]$, with $|G_{xx}|$ being the modulus of the complex autospectrum.

For each test, the sound measurements were performed during 4 min and repeated at least five times. Based on these measurements, the spectral analysis was applied considering an overlap of 50%, a Hanning window, and a frequency resolution of 0.25 Hz. The analysis resulted in a narrowband multispectrum with a time step of 125 ms. It showed that the acoustic measurements were stationary whatever the configuration or the unit discharge. Indeed, as shown in Fig. 3 for a confined model and a unit discharge of 0.03 $m^2 \cdot s^{-1}$, the sound level is constant in time for a fixed frequency. The maximum standard deviation of the sound level in time, for all tests, remains below 7 dB whereas the standard deviation never exceeds 1.5 dB at the characteristic local peak. Therefore, the temporal mean of the multispectrum was calculated for each test. From this mean signal, two parameters were extracted to characterize the oscillations: the maximum sound level and its associated frequency.

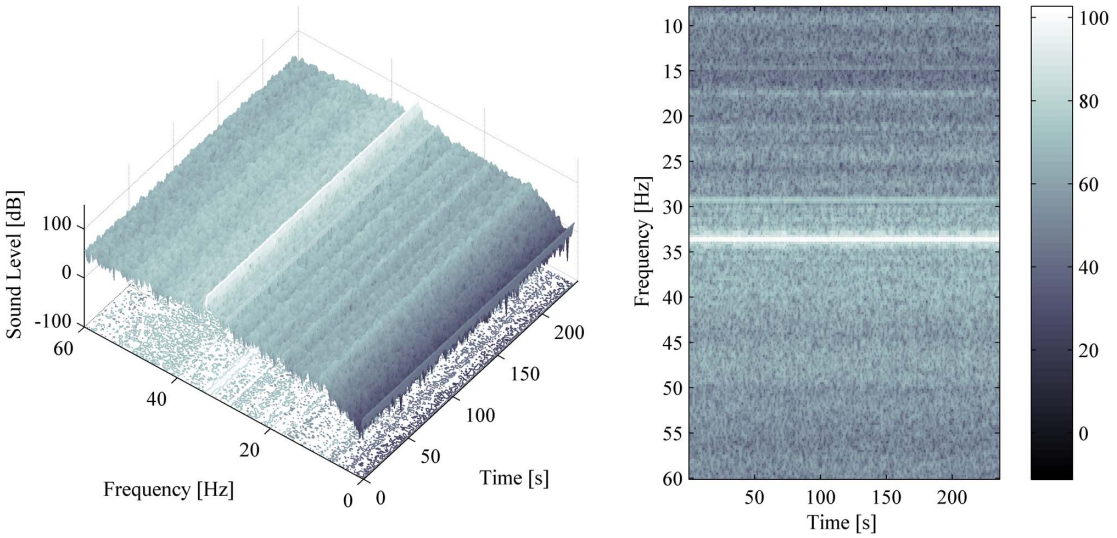

Fig. 3. Multispectrum of audio signal for a confined model and a unit discharge of 0.03 $m^2 \cdot s^{-1}$

J. Hydraul. Eng., 2018, 144(3): 04018001

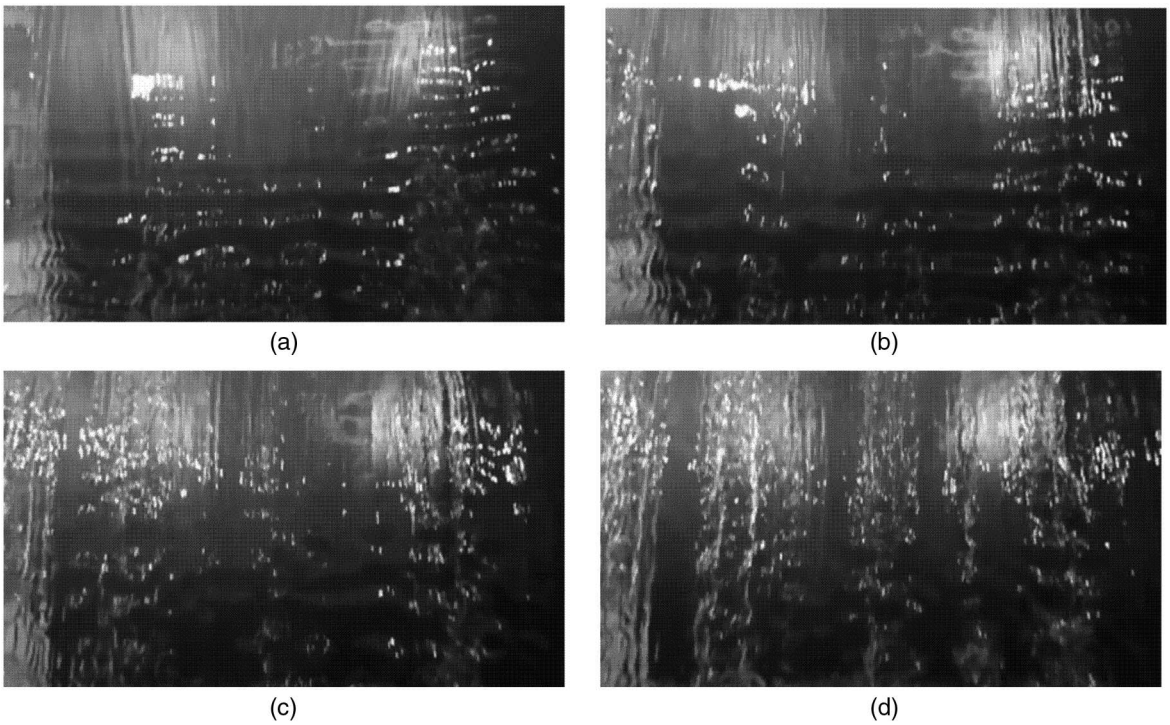

Fig. 4. Nappe visualization for the confined model: (a) 0.015 $m^2 \cdot s^{-1}$; (b) 0.030 $m^2 \cdot s^{-1}$; (c) 0.045 $m^2 \cdot s^{-1}$; (d) 0.06 $m^2 \cdot s^{-1}$ (images recorded with a acquisition frequency of 240 Hz)

Image Analysis

The second method used to characterize the nappe oscillations is based on image analysis. For this purpose, two high-speed cameras, Go-Pro Hero 4 (GoPro, San Mateo, California) and ImagerMX4M Lavision (Lavision, Goettingen, Germany), were available in the laboratory. Because both cameras have an acquisition frequency higher than 200 Hz, according to the Shannon theorem (Shannon 1949), they allow measurement without loss of information for frequencies lower than 100 Hz. Because the frequencies of interest in this study where lower than 60 Hz, both cameras were used indifferently depending on their availability.

Horizontal bands being the visible characteristics of the nappe oscillation phenomenon, the camera was placed along the centerline of the weir crest, 2.5 m downstream in front of the falling nappe. This location allowed to capture the visible horizontal bands on the images of the falling water. Fig. 4 illustrates the flowing nappe for the confined model for four different unit discharges. Oscillations are clearly visible for unit discharges of 0.015 and 0.030 $m^2 \cdot s^{-1}$ whereas the amplitude of oscillations seems to decrease for 0.045 $m^2 \cdot s^{-1}$. For high unit discharges, the horizontal bands appear to be disorganized compared with the ones visible for the lower discharges. In addition, the flow visualization shows the propagation of the oscillations along the nappe according to the flow direction (Fig. 5). It is also observed that the oscillations amplitude is higher at the lower part than at the upper part of the nappe.

Analysis of the images enables the calculation of the frequency of oscillations. Assuming that the horizontal bands were due to the lighting on the undulating surface, the frequency of the bands was determined by the time evolution of data carried by a set of pixels on a succession of images. The method is conceptually sketched in Fig. 6. In this figure, the undulating nappe surface, represented at three successive time steps, shows horizontal bands (lit or unlit bands) moving according to the flow direction. For a fixed image frame, a chosen line of pixels (represented by a thick black line

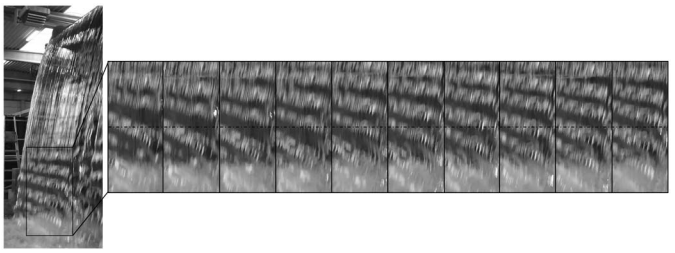

Fig. 5. Downstream side view of the oscillation; tracking of the oscillations along the nappe in a set of 10 successive images, 8.3 ms between the images

in the image frame) carries information which varies in time. The numerical value associated to each pixel depends on whether the pixels are on the illuminated zone of the oscillation or not. This numerical value, for images in gray scale and encoded in 8 bits, is between 0 (white) and 255 (black). Considering the average value on a line of pixels, the oscillation frequency is calculated by the fast Fourier transform (FFT) of its time evolution. In order to illustrate this methodology, an analysis on 600 images (recorded at 240 Hz, i.e., 2.5-s-long movie) is shown in Fig. 7 for the confined model and a unit discharge of 0.045 $m^2 \cdot s^{-1}$. Fig. 7 illustrates (1) the time evolution of a chosen line of 300 pixels; (2) the fluctuation of the average value of this line; and (3) the FFT of this fluctuating signal. A periodic pattern is clearly visible in Fig. 7; even if for the instantaneous image [Fig. 4(c)] the bands are hard to distinguish. The dominant frequency is found equal to 31.6 Hz (Fig. 7).

The resolution of this frequency calculation from images analysis is given by the ratio between the acquisition frequency and the number of snapshots. The acquisition frequency of the camera was either 240 Hz for the Go-Pro Hero4 or 300 Hz for the ImagerMX4M. Image analysis was conducted with the number of

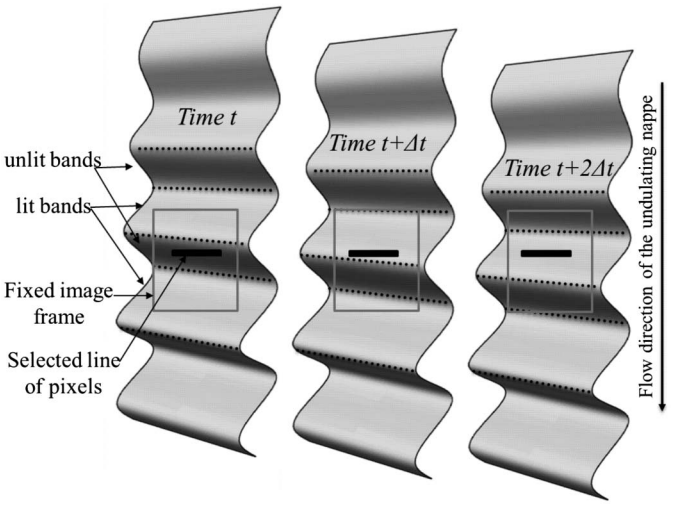

Fig. 6. Conceptual representation for image analysis

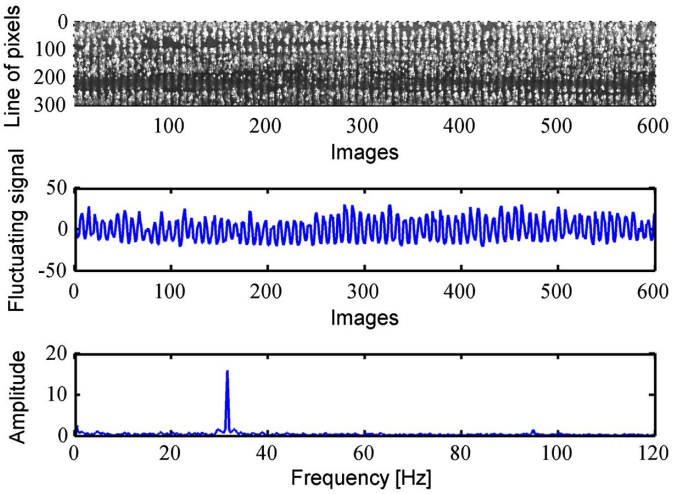

Fig. 7. Steps of image analysis on 600 images for the confined model and a unit discharge of 0.045 $m^2 \cdot s^{-1}$

snapshots needed to get a resolution at least identical to that of sound analysis (0.25 Hz), that is, 960 images for the Go-Pro Hero4 and 1,200 images for the ImagerMX4M. For each test, six lines of 300 pixels were considered per snapshot and at least five sets of images were analyzed. The image analysis, therefore, led to a minimum of 30 calculated points per tested unit discharge.

Results

Nappe Oscillation Occurrence

As already mentioned, nappe oscillation is characterized visually by horizontal bands in the flowing nappe, as displayed in Fig. 4. In addition, intense acoustic pressure waves and the associated noise, that have been aptly described as sounding similar to a helicopter or an amplified bass note (Casperson 1993a), may support the detection of the oscillations. Both flow visualizations and sound measurements are, therefore, analyzed in order to define the flow range affected by the nappe oscillations. Nevertheless, it may happen that only one of these characteristics is detectable. Indeed, for low unit discharges, horizontals bands are predominant although this characteristic disappears faster than the typical noise for higher unit discharges.

Based on qualitative observation, that is, "*Are horizontal bands visible and specific noise audible?*" the range of flow discharge affected by nappe oscillation was first estimated. In the case of the confined model, it was between 0.01 and 0.055 $m^2 \cdot s^{-1}$, and it was between 0.01 and 0.045 $m^2 \cdot s^{-1}$ for the aerated model. Therefore, the range between 0.01 and 0.06 $m^2 \cdot s^{-1}$ was systematically investigated in terms of sound and image analyses.

Besides, various nappe oscillation mitigation solutions were also tested for a confined model. They demonstrated their effectiveness regarding nappe oscillation removal (Lodomez et al. 2016). In this paper, in order to get a reference situation without oscillation, a very effective and simple mitigation technique has been considered: a continuous step along the entire width of the weir added at the downstream edge of the crest. Results gained with this solution are presented in Figs. 8 and 9 by comparison with the same configuration without countermeasure. These figures illustrate the absence of the two nappe oscillation characteristics, namely a horizontal banding and a local peak in the sound signal.

Sound Analysis

The mean autospectra extracted from sound measurements are typically of two types, as illustrated in Fig. 10 for a confined model and two different unit discharges. Fig. 10(a) shows, for a unit discharge of 0.03 $m^2 \cdot s^{-1}$, a spectrum in which a clearly visible peak in sound level appears for a specific frequency, whereas for 0.06 $m^2 \cdot s^{-1}$ there is no obvious dominant peak. For a unit discharge of 0.03 $m^2 \cdot s^{-1}$, nappe oscillations appear and are characterized by a sound level up to 100 dB. This maximum quantifies the magnitude of the phenomenon whereas the frequency of oscillations, 33.25 Hz, is directly given by the associated frequency of the peak in the audio spectrum. For a unit discharge of 0.06 $m^2 \cdot s^{-1}$, nappe oscillations are weak or nonexistent because

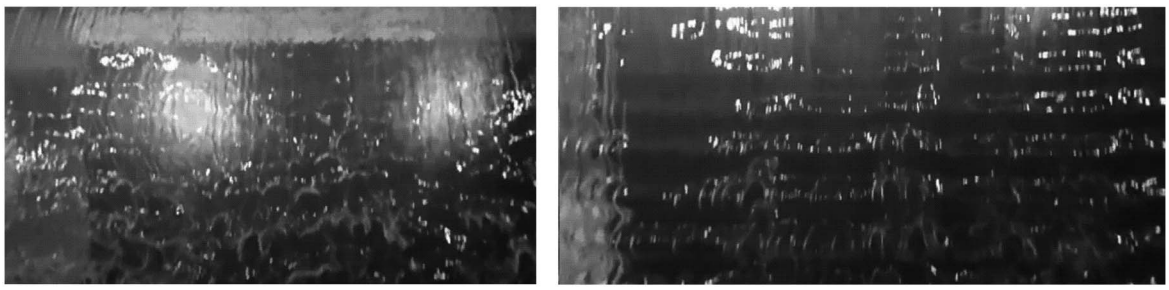

Fig. 8. Flow visualization of the nappe for a confined model and 0.02 $m^2 \cdot s^{-1}$: (a) with a mitigation technique; (b) without mitigation

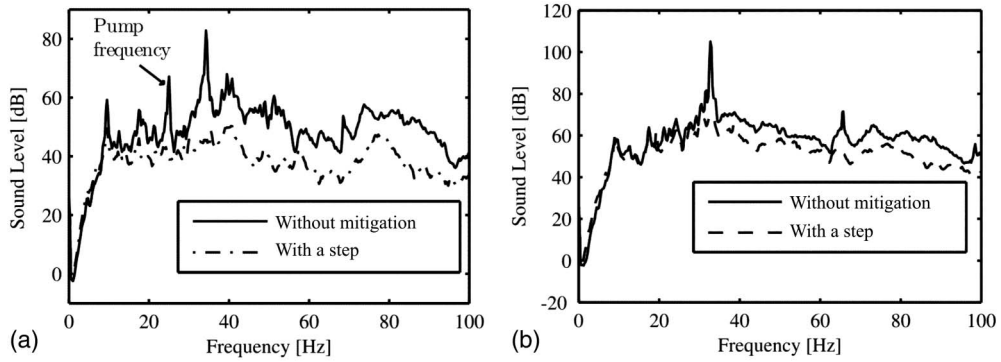

Fig. 9. Mean autospectrum of sound measurement for a confined model with and without mitigation technique for (a) 0.015 $m^2 \cdot s^{-1}$; (b) 0.045 $m^2 \cdot s^{-1}$

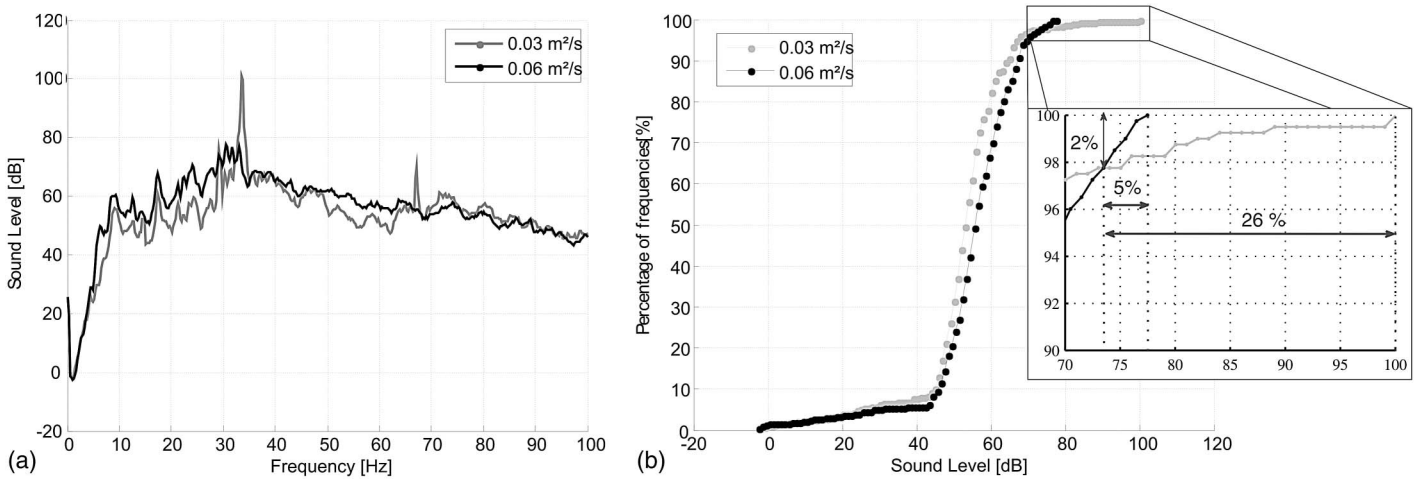

Fig. 10. (a) Mean autospectrum of sound measurement for a confined model; (b) the corresponding cumulative frequencies of the mean auto spectrum

there is no local maximum in the mean autospectrum. The distinction between these two examples is illustrated in Fig. 10(b) by the cumulative frequencies of the mean autospectra, which exemplifies the concept of "dominant" peak. For the unit discharge of 0.03 $m^2 \cdot s^{-1}$, 2% of the frequencies increase the sound level by 26% whereas for the nonoscillating configuration (0.06 $m^2 \cdot s^{-1}$) the frequencies distribution over the sound level is more uniform.

The detection of a dominant peak for the confined model between 0.01 and 0.055 $m^2 \cdot s^{-1}$ and for the aerated model between 0.01 and 0.045 $m^2 \cdot s^{-1}$ is in agreement with the detection of nappe oscillation using the coupling of a qualitative audible and visual detection. In these flow ranges, the peak sound frequency varies between 31.5 and 35 Hz for the confined model. For the aerated model, a constant frequency of 35.25 Hz was observed between 0.025 and 0.04 $m^2 \cdot s^{-1}$. It was 45–50 Hz for lower unit discharges. For unit discharge higher than 0.04 $m^2 \cdot s^{-1}$, the frequency was equal to 45 Hz.

Image Analysis

The flow range for which oscillations are visible corresponds to the one defined by acoustic measurements. Nevertheless, it is found that the visual characteristics are more pronounced for low unit discharges whereas the noise increases for larger unit discharges in the affected flow range. The image analysis was applied to the confined model and the aerated model for the same unit discharge range as for the sound analysis. Results are presented in Table 1 as the mean, minimum, and maximum frequencies resulting from a minimum of 30 data per discharge (except for one discharge). The frequency of the nappe oscillations did not change by more than 2.5 Hz for the aerated model and unit discharge between 0.025 and 0.04 $m^2 \cdot s^{-1}$. The mean oscillation frequency was 36.3 Hz in this range whereas for lower unit discharges, between 0.01 and 0.02 $m^2 \cdot s^{-1}$, it was equal to 50.61 Hz. For the confined model, the frequency of the oscillations was between 31.25 and 34 Hz for a unit discharge varying between 0.015 and 0.045 $m^2 \cdot s^{-1}$. In contrast, a frequency of 39 Hz was observed for a unit discharge of 0.01 $m^2 \cdot s^{-1}$.

Discussion

The audio signal of nappe oscillations is characterized by a local peak in the mean autospectrum. The oscillations are not the only process able to create such a peak. In particular, the pumps used to feed the model in the laboratory induce a sound peak at the frequency of the pump rotation. As an example, the second maximum of the mean autospectrum for the configuration without mitigation in Fig. 9(a) is due to the pump rotating at a 25-Hz frequency. To overcome this problem, in every test, special care was paid to adapt the pump frequency so that it did not affect the mean autospectrum

Table 1. Frequencies from the Image Analysis for the Confined and the Aerated Models

Aerated model					Confined model				
Unit discharge ($m^2 \cdot s^{-1}$)	Frequency (Hz)			Number of data	Unit discharge ($m^2 \cdot s^{-1}$)	Frequency (Hz)			Number of data
	Mean	Maximum	Minimum			Mean	Maximum	Minimum	
0.010	50.76	50.8	50.75	36	0.010	39.12	39.25	39	30
0.015	50.52	50.60	50.49	42	0.015	34.25	34.27	34.25	30
0.020	50.56	50.65	50.5	48	0.020	34.46	34.5	34.38	36
0.025	36.24	36.25	36.2	54	*0.025*	*33.56*	*33.63*	*33.5*	*12*
0.030	36.27	36.3	36.25	30	0.030	31.25	31.27	31.24	30
0.035	35.10	35.25	35	30	0.035	33.68	33.75	33.6	30
0.040	35.42	36	35	36	0.040	31.5	31.5	31.5	30
0.045	37.46	41.75	37.7	42	0.045	31.52	31.6	31.5	30

Note: Line of 300 pixels, six lines per frame, a minimum of 0.25 Hz fast Fourier transform resolution, and a minimum of five image sets were used [except for the confined model and a unit discharge of 0.025 $m^2 \cdot s^{-1}$ (in italics) due to a lack of robust data].

in the frequencies of the nappe oscillations. In addition, when repeating the tests, different pump frequencies were used to isolate unequivocally the sound signal from the oscillations. Therefore, all the intensities and associated frequencies of mean autospectra given in this paper are unequivocally related to the nappe oscillation.

In the description of the sound analysis methodology, it has been assumed that the oscillation's noise results from the action of the nappe on the surrounding air and not from the impact on the apron. To verify this assumption, measurements were carried out with the aerated model by adding on the top of the concrete apron two 4-cm-thick synthetic horsehair panels. The resulting 8-cm-thick mattress modified the impact conditions and in particular smoothen the noise. Fig. 11 illustrates the audio spectra acquired with and without this modified configuration of the zone of impact for a discharge of 0.02 $m^2 \cdot s^{-1}$. It can be observed that the main peak in sound level appears in both cases for the same frequency and a very similar amplitude. With the modification of the impact area, the harmonics of this main peak frequency are still visible whereas sound level is globally more uniform. These results confirm the hypothesis that the sound generated by the nappe oscillations originates from an action of the falling sheet of water on the surrounding air and is not merely related to the impact of the nappe.

In Fig. 12, the intensity of the highest peak in the mean autospectrum is plotted as a function of the unit discharge for the aerated weir and the confined weir with and without a mitigation measure. The resulting graph shows, for both configurations experiencing nappe oscillations (aerated and confined ones), a sound level evolution in four successive phases: growing, maximum intensity stabilization, damping, and finally a new stabilization phase (Fig. 13). The occurrence of nappe oscillations is related to the first three stages which are bounded by the discharges leading to a local dominant peak in the audio spectrum and horizontal bands in flow visualization. In contrast, the sound level for the confined model with a mitigation technique evolves monotonously with the discharge. The comparison between the marks for the confined and the aerated weir shows a sound intensity of the oscillations higher in case of confinement and a little bit more important range of affected discharges (Fig. 12). In addition, for the aerated model, the data are more scattered than for the confined configuration. This first finding is in agreement with the assumption of Casperson (1993b) regarding the amplification effect of the confinement.

The frequency associated to the sound data of Fig. 12 is plotted as a function of the unit discharge in Fig. 14 for the confined and aerated model. Beyond the flow range affected by nappe oscillation, the sound peak frequency is meaningless because there is no oscillation. Again, the results are more scattered in case of the aerated model. However, three frequency levels are clearly visible: the frequency associated to low discharges is rather constant at 50 Hz whereas frequencies of 36 and 43 Hz are observed for the higher discharges. These three frequencies have a constant

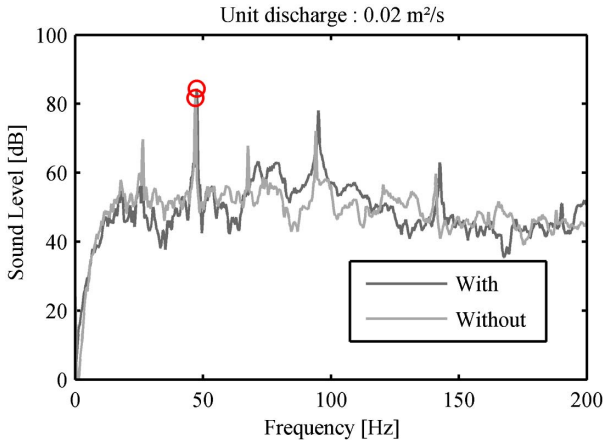

Fig. 11. Mean autospectrum of sound measurement for an aerated configuration with a modification of the apron with synthetic horsehair panels and without modification, that is, concrete apron

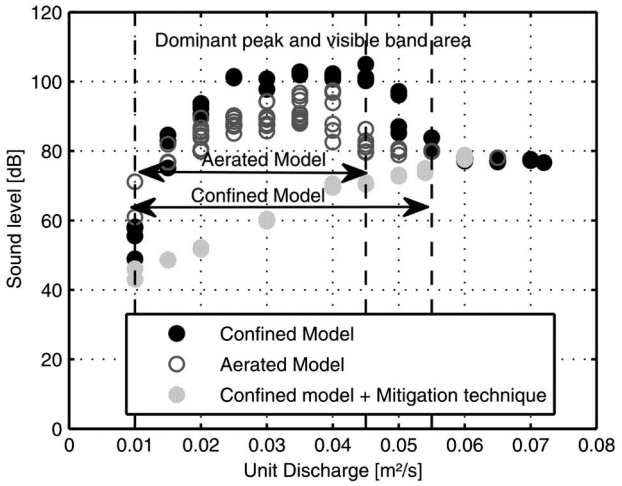

Fig. 12. Results of sound analysis for configurations: confined model, aerated model, and confined model with a mitigation technique

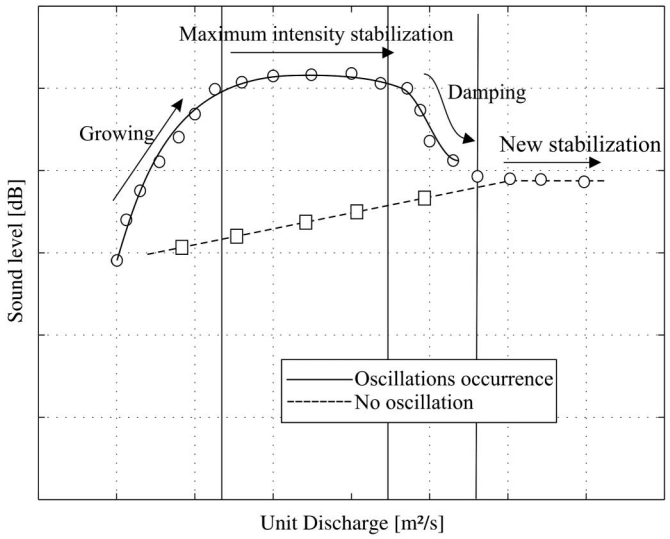

Fig. 13. Typical evolution of the highest peak intensity in the mean autospectrum as a function of the unit discharge for oscillating and non-oscillating nappes

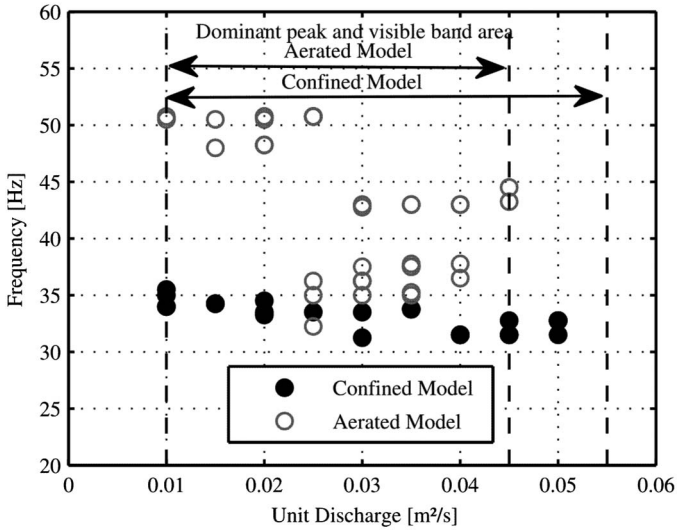

Fig. 14. Sound frequency associated to the main peak of the autospectrum

difference of 7 Hz. On the contrary, results for the confined configuration are almost constant because the results variability is only 2.5 Hz with a mean value of 33 Hz. Again, the confinement helps in stabilizing the oscillations, but is not a requisite to produce them.

The results obtained by the sound and the image analysis are compared in terms of frequencies in Fig. 15. This figure shows that for a given unit discharge, both methodologies give the same frequency of oscillation to the uncertainty of the measurements, especially in case of confined model. For the aerated model, the image analysis provides only one of the two levels of frequency for a given unit discharge. This could be explained by the fact that some sound and images measurements were not made simultaneously.

In order to compare the results presented in this paper with the ones from the literature, a dimensionless frequency f_{ad} and the Reynolds number R have been used. They are defined by the following equations:

$$f_{ad} = \frac{q}{f e^2} \quad \text{and} \quad \mathsf{R} = \frac{q}{\nu} \tag{2}$$

where q = specific discharge (in square meters per second); e is a characteristic dimension of the nappe (in meters); f = nappe oscillation frequency (per second); and ν = kinematic viscosity (in square meters per second). The characteristic dimension e was chosen as the nappe thickness at the impact, calculated from the downward velocity of the water sheet $v(y)$ at the impact defined following Casperson (1993a):

$$e = \frac{q}{v_y(L)} = \frac{q}{\sqrt{v_0^2 + 2gL}} \tag{3}$$

where v_0 = vertical velocity of the sheet leaving the crest or the slot (in meters per second); L = chute height (in meters); and g = gravity acceleration (in square meters per second). Contrary to the flow from a vertical slot, the initial velocity for the flow over a weir is supposed to be purely horizontal, that is, v_0 equal 0.

Fig. 16(a) shows the dimensionless frequencies obtained for the confined model as a function of the Reynolds number. The experimental results from Binnie (1972), Casperson (1993a), and Schmid and Henningson (2002) have also been added. Although the range of Reynolds number of the data from this study differs by one order of magnitude of the one from previous researches, and although the flow initial conditions are varied (vertical slot in a pressurized tube versus free-surface weir), all the data align quite well along the same tendency curve. The recent data of Anderson (2014),

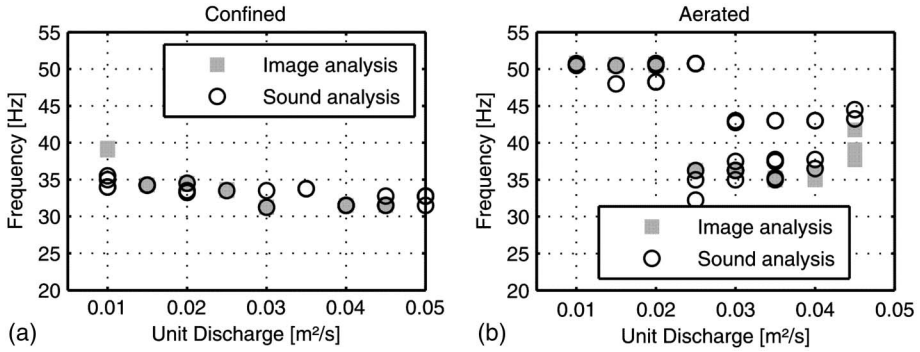

Fig. 15. Comparison of the frequencies from sound and image analyses: (a) for the confined model; (b) for the aerated model

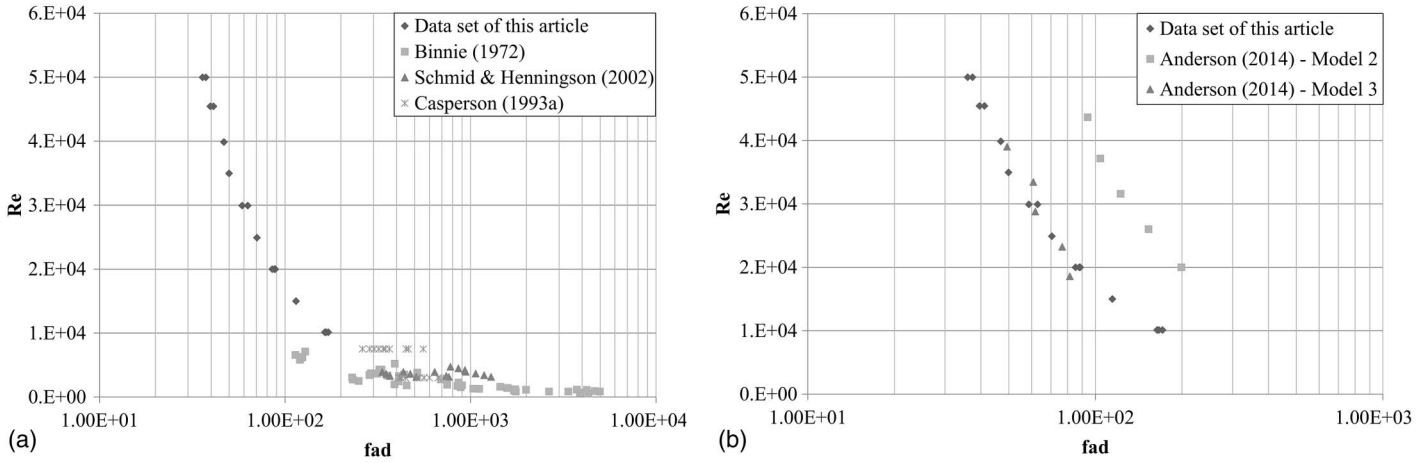

Fig. 16. Dimensionless frequency of nappe oscillation for various data sets as a function of the Reynolds number

acquired in the same R and crest geometry conditions [Anderson (2014) Model 3], collapse with the data from this study [Fig. 16(b)]. On the contrary, data acquired in the same R conditions but with a modified crest shape [Anderson (2014) Model 2] follow the same tendency but with a shift in frequency [Fig. 16(b)]. This comparison suggests that oscillations observed in flow nappes falling vertically from a pressurized slot or originating from a free-surface weir are the expression of the same physical phenomenon. It also shows that, at constant discharge, the initial flow characteristics impact the oscillations frequency.

Conclusions

A comprehensive methodology based on sound and images analysis has been proposed to characterize the frequency and the noise of the oscillations of free falling nappe. Their application on a 1:1 physical model of a free-surface linear weir enables to characterize the development of oscillations of the downstream nappe and to identify the range of discharges affected. The experimental results show that the presence of air confined behind the nappe does not affect the occurrence of oscillations but that it acts as an amplification and stabilization factor. They also show the obvious link between the nappe oscillations and the associated noise, suggesting that the sound is generated by the oscillations' action on the surrounding air and not by the impact of the nappe on the ground. This has also been verified by modifying the rigidity of the impact apron.

Finally, comparison on a dimensionless basis of the data from this study with experimental data from the literature suggests that oscillations observed in flow nappes falling vertically from a pressurized slot or originating from a free-surface weir are the expression of the same physical phenomenon. It also shows that, at constant discharge, the initial flow characteristics impact the oscillations frequency. Although not enough data are available yet to support this assumption, one can assume that the pressure distribution in the nappe plays a role in the oscillation development. This could indeed explain the variation of the dimensionless frequencies observed in both cases of nappes originating from free-surface weirs, where the weir geometry influences directly the bottom pressure at the detachment point, and nappes originating from slots in a pressurized tube, that is, positive pressures on both sides of the nappe at the origin. The study is still ongoing in order to identify which of the initial flow parameters affect the oscillation.

Acknowledgments

The authors are grateful for the construction of the physical model to the technicians of HECE-ULg. They also greatly acknowledge B.P. Tullis (UWRL, Utah State University) and B.M. Crookston (Schnabel Eng.) for the fruitful discussions about nappe oscillations.

Notation

The following symbols are used in this paper:

e = characteristic length (m);
f = oscillation frequency (s^{-1});
f_{ad} = dimensionless frequency;
g = gravity acceleration ($m \cdot s^{-2}$);
L = fall height (m);
q = specific discharge ($m^2 \cdot s^{-1}$);
R = Reynolds number;
T_f = falling time (s);
ν = kinematic viscosity ($m^2 \cdot s^{-1}$);
v_0 = initial vertical velocity ($m \cdot s^{-1}$); and
W = Weber number.

References

01dB-Metravib version 9.4 [Computer software]. ACOEM, Limonest, France.

Anderson, A. A. (2014). "Causes and countermeasures for nappe oscillation." Master's thesis, Utah State Univ., Logan, UT.

Binnie, A. (1972). "The stability of a falling sheet of water." *Proc., Royal Society of London A: Mathematical, Physical and Engineering Science*, The Royal Society, London, 149–163.

Binnie, A. (1974). "Resonating waterfalls." *Proc., Royal Society of London A: Mathematical, Physical and Engineering Science*, The Royal Society, London, 435–449.

Casperson, L. W. (1993a). "Fluttering fountains." *J. Sound Vibr.*, 162(2), 251–262.

Casperson, L. W. (1993b). "Fluttering fountains: Simplified models." *J. Appl. Phys.*, 74(8), 4894–4898.

Casperson, L. W. (1994). "Fluttering fountains: Stability criteria." *J. Appl. Phys.*, 75(10), 4892–4894.

Chanson, H. (1996). "Some hydraulic aspects during overflow above inflatable flexible membrane dam." *Rep. CH47/86*, Univ. of Queensland, Brisbane, Australia.

Crookston, B. M., Anderson, A., Shearin-Feimster, L., and Tullis, B. P. (2014). "Mitigation investigation of flow-induced vibrations at a rehabilitated spillway." *Proc., 11th National Conf. on Hydraulics in Civil Engineering and 5th Int. Symp. on Hydraulic Structures: Hydraulic Structures and Society-Engineering Challenges and Extremes*, Engineers Australia, Barton, Australia, 149–156.

Crookston, B. M., and Tullis, B. (2013). "Hydraulic design and analysis of labyrinth weirs. I: Discharge relationships." *J. Irrig. Drain. Eng.*, 10.1061/(ASCE)IR.1943-4774.0000558, 363–370.

Curle, N. (1953). "The mechanics of edge-tones." *Proc., Royal Society of London A: Mathematical, Physical and Engineering Sciences*, The Royal Society, London, 412–424.

dBFA version 4.9 [Computer software]. 01dB Metravib, Limonest, France.

De Rosa, F., Girfoglio, M., and de Luca, L. (2014). "Global dynamics analysis of nappe oscillation." *Phys. Fluids*, 26(12), 122109.

Girfoglio, M., De Rosa, F., Coppola, G., and de Luca, L. (2017). "Unsteady critical liquid sheet flows." *J. Fluid Mech.*, 821, 219–247.

Helmholtz, H. V. (1868). *Ueber die Thatsachen, die der Geometrie zum Grunde liegen*, Nachrichten von der Königl. Gesellschaft der Wissenschaften und der Georg-Augusts-Universität zu Göttingen, Göttingen, Germany, 193–221.

Lodomez, M., Crookston, B. M., Tullis, B. P., Pirotton, M., and Erpicum, S. (2016). "Nappe vibration mitigation techniques for free-overfall structures." *Hydraulic Structures and Water System Management, 6th IAHR Int. Symp. on Hydraulic Structures*, B. Crookston and B. Tullis, eds., Portland, OR, 359–366.

Metropolitan Water, Sewerage, and Drainage Board. (1980). "Investigation into spillway discharge noise at Avon Dam." *ANCOLD Bull.*, 57, 31–36.

Naudascher, E., and Rockwell, D. (1994). *Flow-induced vibrations: An engineering guide*, A.A. Balkema, Rotterdam, Netherlands.

Naudasher, E. (1965). "Discussion on nappe oscillation." *Proc. ASCE, J. Hydraul. Div.*, May.

Petrikat, I. K. (1958). "Vibration tests on weirs and bottom gates, part one." *Water Power*, 10, 52–57.

Sato, Y., Miura, S., Nagamine, T., Morii, S., and Ohkubo, S. (2007). "Behavior of a falling water sheet." *J. Environ. Eng.*, 2(2), 394–406.

Schmid, P. J., and Henningson, D. S. (2002). "On the stability of a falling liquid curtain." *J. Fluid Mech.*, 463, 163–171.

Schwartz, H. I. (1964). "Projected nappes subject to harmonic pressures." *Proc. Inst. Civ. Eng.*, 28(3), 313–326.

Schwartz, H. I. (1966). "Edgetones and nappe oscillation." *J. Acoust. Soc. Am.*, 39(3), 579–582.

Shannon, C. E. (1949). "Communication in the presence of noise." *Proc. IRE*, 37(1), 10–21.

Squire, H. (1953). "Investigation of the instability of a moving liquid film." *Br. J. Appl. Phys.*, 4(6), 167–169.

USBR (United States Bureau of Reclamation). (1964). "Experience of the Bureau of Reclamation with flow-induced vibrations." *Rep. No. 538*, Washington, DC.